Journal of Marine Research, 59, 29–51, 2001

Particle trapping in a stratified flood-dominated estuary

by Robert J. Chant[1] and Allan W. Stoner[2,3]

ABSTRACT

Observations in the Navesink River estuary in northern New Jersey demonstrate that buoyancy augments the particle trapping tendencies of flood-dominated systems because these estuaries heighten tidal period asymmetries in stratification. During the long and slow ebb which typifies flood-dominated systems, a positive feedback between tidal straining and weak vertical mixing stratifies the estuary. In contrast, during flood, turbulence generated by the stronger tidal currents augments overstraining of the density field and the water column becomes well mixed. The tidal period asymmetries in stratification have profound effects on the vertical structure and transport of suspended matter. During ebb, weak vertical mixing allows suspended material to settle downward. In contrast, strong turbulence during flood mixes suspended matter into the water column where it is transported up estuary. Furthermore, observations reveal that resuspension events are marked by multiple turbidity spikes, suggestive of multiple, limited layers of erodible material. The transport of the turbid waters is consistent with horizontal advection modified by horizontal dispersion. Periods of enhanced stratification are also marked by relatively low levels of turbidity during the ebb, consistent with more complete settling of suspended material following times of high river discharge.

The interplay between buoyancy and tidal asymmetries are further elucidated with a one-dimensional numerical model featuring a turbulent closure scheme and a passively settling tracer. Model results are generally consistent with the field observations, both emphasizing the robust particle trapping tendencies of a stratified flood-dominated estuary. We speculate that enhanced particle trapping following times of high river discharge may have important biological consequences.

1. Introduction

In estuarine systems the interplay between resuspension, mixing and circulation can concentrate suspended matter into zones with elevated levels of turbidity. For example, the turbidity maximum described by Schubel (1968) and Schubel and Pritchard (1972) occurred in the upper reaches of the Chesapeake Bay where material in the lower layer accumulates due to horizontal flow convergence at the head of the salt wedge, where gravitationally driven landward flow vanishes. Young and Rhoads (1971), Rhoads (1973)

1. Institute of Marine and Coastal Sciences, Rutgers University, New Brunswick, New Jersey, 08901, U.S.A. ***email: chant@imcs.rutgers.edu***

2. Northeast Fisheries Science Center, National Marine Fisheries Service, 74 Magruder Road, Highland, New Jersey, 07732, U.S.A.

3. Present address: Alaska Fisheries Science Center, National Marine Fisheries Service, 2030 S. Marine Science Drive, Newport, Oregon, 97365, U.S.A.

and Rhoads *et al.* (1984) describe high levels of near-bottom turbidity due to resuspension of bottom muds. While the highest levels of turbidity are found in the lowest 2–3 meters of the water column (Rhoads, 1973), turbidity levels are, in general, enhanced beneath the thermocline (Rhoads *et al.,* 1984) due to trapping of particles by stratification. The suspended load in the bottom layer also exhibits a seasonal cycle with peak concentrations occurring as the water column warms between May and July (Rhoads *et al.,* 1984). Sediments on the bottom and suspended in the water column provide an important pathway linking biological and physical processes (Rhoads and Young, 1970; Young and Rhoads, 1971; Rhoads, 1973).

The trapping of suspended material in the vicinity of a salt front has been discussed more recently by Geyer (1993). Upstream of a salt front, turbulence is uninhibited by stratification and thus maintains a suspended load in the water column that is advected seaward by the river flow. Downstream, however, turbulence is suppressed by stratification, and particles settle into a bottom mixed layer. Once in the bottom mixed layer, suspended material is transported landward by gravitational circulation where it accumulates at the foot of the front. In contrast, based on two-dimensional numerical simulations, Burchard and Baumbert (1998) suggest that a turbidity maximum does not require a spatially variable mixing but rather can be maintained by converging estuarine flows in the presence of a spatially and temporally constant vertical eddy diffusivity. However, while a constant vertical mixing may produce a turbidity maximum, it will not capture intratidal variations of the suspended load associated with tidal period variations in vertical mixing.

Tidal period variations in mixing occur, in part, due to the straining of the horizontal density field (van Aken, 1986) by the vertically sheared oscillating tide (Simpson *et al.,* 1990; Linden and Simpson, 1988). This interaction, referred to as tidal straining (Simpson *et al.,* 1990), produces stronger mixing on flood, when vertical shear acting on the horizontal density gradient destabilizes the water column, then on ebb, when shear stratifies the water column. Tidal period asymmetries in vertical mixing is apparent in microstructure profiles (Peters and Bokhorst, 2000) and plays a fundamental role in the tidally averaged dynamics (Jay and Smith, 1990). Asymmetries in vertical mixing also drive tidal period fluctuations in the suspended load (Jay and Musiak, 1994). For example, Lang *et al.* (1989) suggest that observed tidal period variability in turbidity is related to tidal period variations in resuspension and deposition, which in turn are related to tidal period asymmetries in vertical mixing. The importance of resuspension and deposition is also suggested by Wellerhaus (1981) and Hamblin (1989). More recently, Friedrichs *et al.* (2000) show that tidal period asymmetries in vertical mixing due to tidal straining produces flood to ebb asymmetries in the suspended load, driving a net landward sediment load and trapping fine grain sediments within the estuary.

Other processes also trap material within estuaries. For example, Officer (1981) described such a mechanism by noting that tidal currents tend to be strongest at the mouth of an estuary. Particles resuspended on the flood are transported up estuary where they settle during slack water in regions of reduced tidal energy. In contrast, particles

resuspended on ebb are carried seaward to regions of enhanced tidal energy where they are resuspended and transported back up estuary on the following flood. This trapping mechanism can be augmented by barotropic tidal asymmetries, particularly if the estuary becomes flood-dominated (Speer and Aubrey, 1985; Friedrichs and Aubrey, 1988; Friedrichs and Madsen, 1992). Barotropic tidal asymmetries are generated by nonlinear dynamics and characterized by unequal times of rising and falling tides. A flood-dominated estuary fills faster than it empties, while ebb-dominated systems empty more quickly. Systems become flood-dominated when the tidal range is greater than 20 percent of the mean water depth; ebb dominance occurs when high water storage along the flanks of an estuary represents an appreciable fraction of the tidal prism (Speer and Aubrey, 1985; Friedrichs and Madsen, 1992). Tidal asymmetries can be quantified by the ratio and relative phase of the M2 and M4 tidal constituents (Friedrichs and Aubrey, 1988), where the M2 is the principal semidiurnal tidal constituent, with a period of 12.42 hours, and the M4 its first harmonic, with a period of 6.21 hours. Higher harmonics, such as the sixth diurnal, M6, and eighth diurnal, M8, with periods of 4.14 and 3.11 hours, respectively, are also generated, and contribute to barotropic tidal asymmetries.

Flood-dominated systems tend to be shallow and are often described by depth-averaged dynamics. Consequently, little attention has been paid to the effects of buoyancy in flood-dominated systems. Nevertheless, Geyer (1997) has shown that strong stratification can occur in an estuary with a mean depth less than 2 meters.

In this paper we discuss the interaction between buoyancy, barotropic tidal asymmetries and suspended material in a flood-dominated system. The description is based on a blend of observations and numerical simulations. Results emphasize that trapping in flood-dominated systems is augmented by river discharge. Finally, we speculate the role that these physical processes play on recruitment.

2. Study site

The Navesink River estuary is located in northern New Jersey just south of Raritan Bay (Fig. 1). Though it is small, 10 km in length, and shallow, average depth $\sim$2 m, its dimensions typify those of many of the small tributaries along the US east coast and throughout the world. A deeper channel runs along the northern side of the estuary, where the depth exceeds 5 m in channel contractions. A wide flank occupies the middle and southern portion of the channel. Tides in this system are primarily semidiurnal, with a mean range of over 1 m, and are strongly flood-dominated. Buoyancy is provided at the head by the Swimming River, a controlled river which provides a mean annual discharge of 2 m^3/s. River discharge, however, can exceed 50 m^3/s following heavy rains.

3. Field program

Field observations were made in spring 1998 to study the tidal dynamics and aspects of the time-varying turbidity field in the central Navesink River estuary (Fig. 1). The field

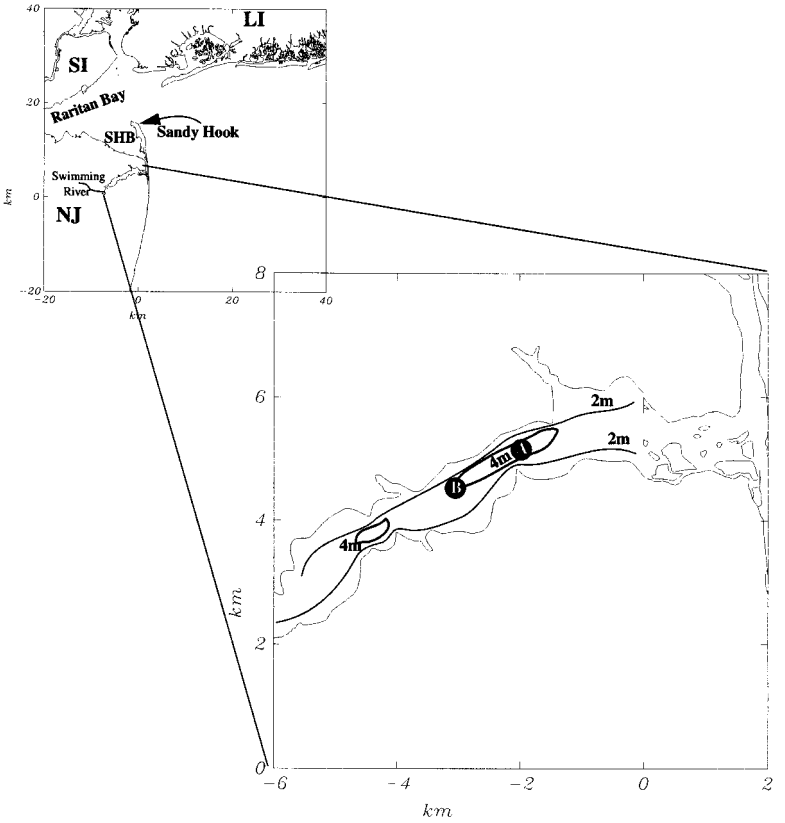

Figure 1. Abbreviations in large scale map are LI—Long Island, SI—Staten Island, NJ—New Jersey, SHB—Sandy Hook Bay. Small scale map shows the study area in the Navesink, the 2 m and 4 m isobath and locations of mooring. Mooring A consisted of an Aanderaa RCM-9 current meter and a paroscientific pressure sensor. Mooring B contained an S4 current meter.

experiment included moored instruments and shipboard observations. Moorings were deployed between March 23 and April 19, 1998. The mooring array consisted of a parascientific pressure sensor and an Aanderaa RCM9 current meter at mooring A, and an S4 current meter at mooring B. Both the RCM9 and S4 measured current vectors, temperature, conductivity and turbidity and both instruments were calibrated by the manufacturer prior to deployment. Pressure is used as a proxy for sea level, although these records also contain additional contributions associated with variations in the depth-averaged fluid density and changes in atmospheric pressure. Daily mean discharge from Swimming River and hourly sea level observations from the northern tip of Sandy Hook were obtained by the US Geological Survey and the National Ocean Service, respectively.

Shipboard measurements were made during the last week of March into the first week of April 1998 and consisted of towing a 1200 kHz RDI Acoustic Doppler Current Profiler while profiling with a Seabird CTD. Position was recorded with differential GPS. The physical observations focused on a region over which there are strong gradients in tidal

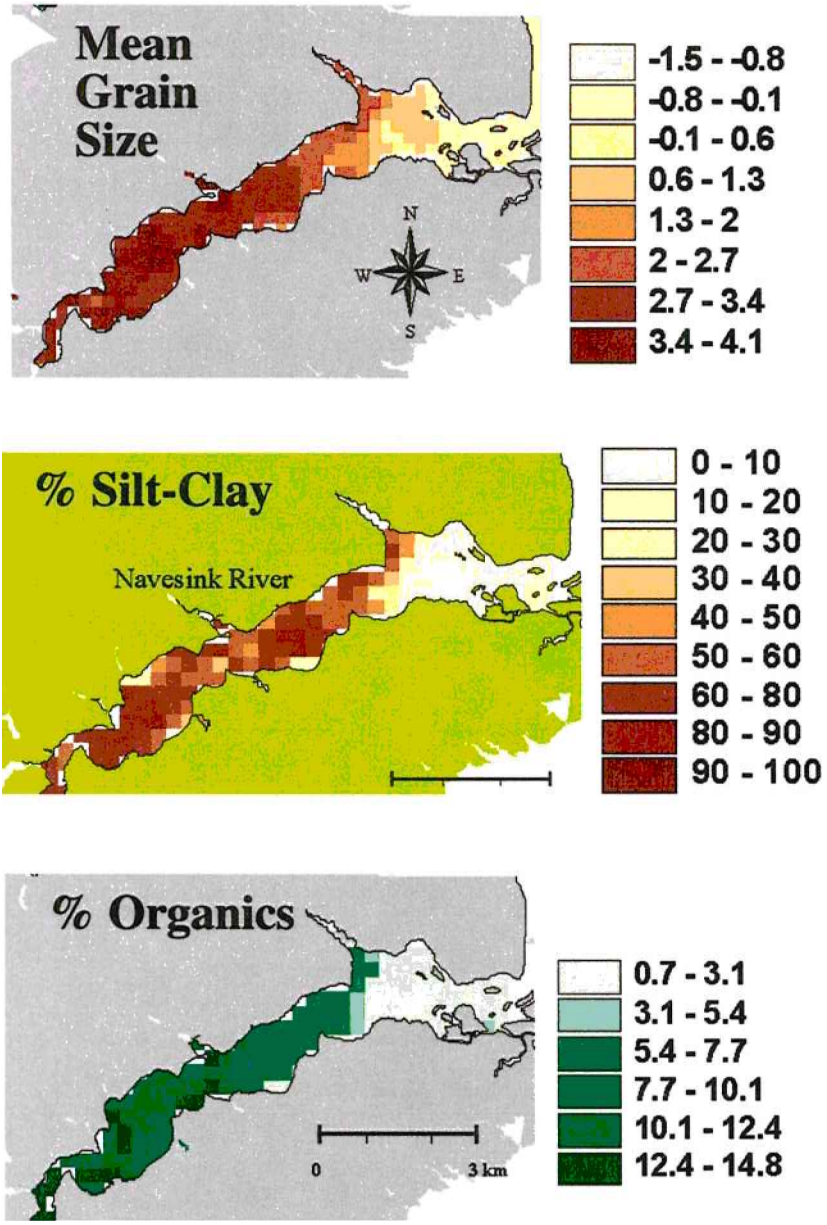

Figure 2. Sediment characteristics. Upper panel, Mean grain size (ϕ); Middle panel % silt and clay; Lower panel % organics. Note change in sediment characteristics over survey region.

current velocity and corresponding sediment characteristics (Fig. 2). The field program occurred following a period of relatively high river discharge which exceeded 10 m^3/s for nearly a week just prior to the field work (Fig. 3). Discharge for the month of March 1998 was 8 m^3/s, approximately twice the average daily discharge during the month of March

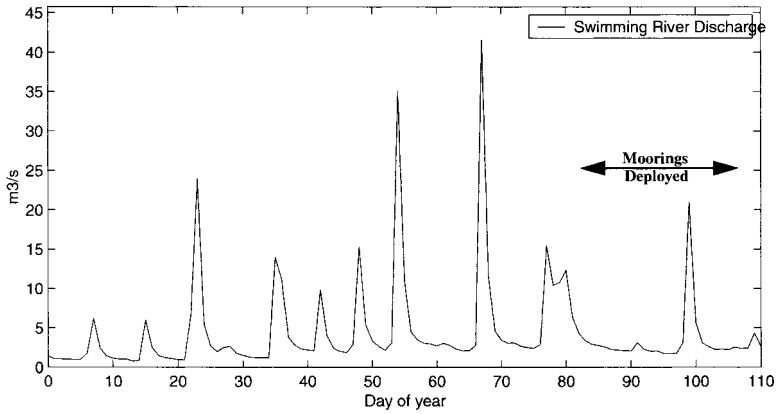

Figure 3. Swimming River daily mean discharge.

between years 1922–1998. Maximum spring tide occurred on March 27, minimum neap tides occurred on April 3.

4. Results

a. Observations

Figure 4 presents sea level at Sandy Hook together with pressure obtained at mooring A. While evidence of flood-dominance is apparent at Sandy Hook, this distortion grows as the tidal wave propagates through Sandy Hook Bay and into the Navesink. The pressure record clearly demonstrates that the estuary fills more quickly than it empties. Tidal constituents obtained from mooring A over the entire record reveal that the ratio between the semidiurnal constituent, M2, and the quarterdiurnal constituent, M4, is 0.1 while the phase lag (2M2 − M4) is 60 degrees, indicating that the Navesink is indeed a strongly flood-dominated system (Friedrichs and Aubrey, 1988).

This ratio, and thus the tidal asymmetry, is modulated by the spring to neap cycle (Fig. 5a). While the semidiurnal range (i.e., the tidal range) varies by a factor of two over

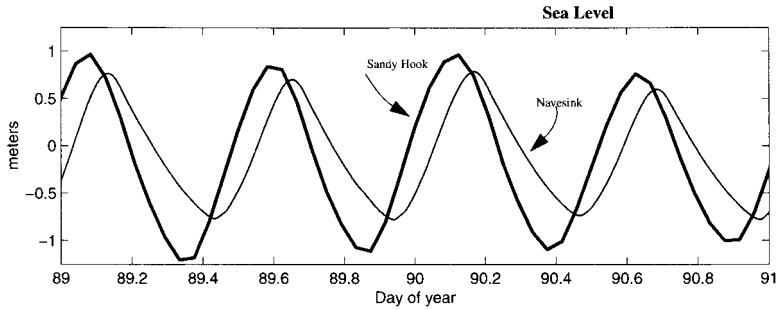

Figure 4. Demeaned sea level from Sandy Hook (thick line) and pressure (thin line) from mooring A.

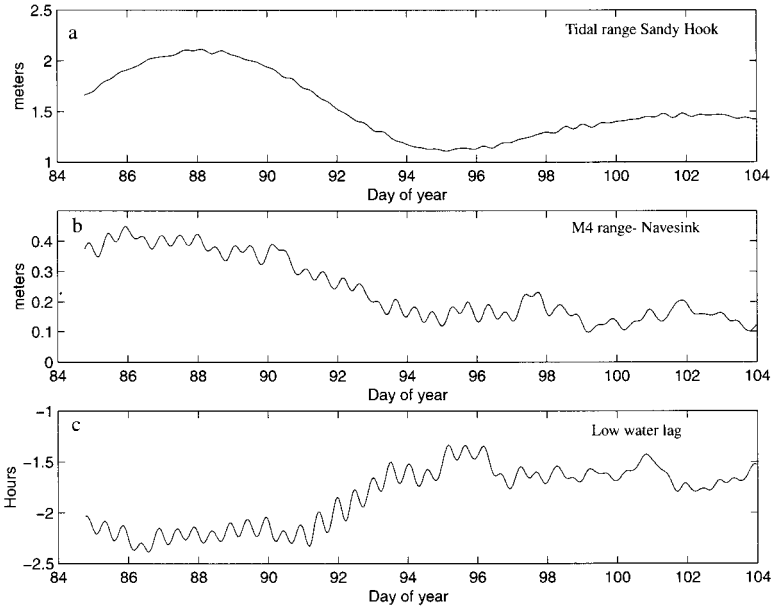

Figure 5. (a) Tidal range at Sandy Hook obtained by demodulating Sandy Hook sea level data at a period of 12.42 hours. (b) Range of quarterdiurnal tide in the Navesink obtained by demodulating the pressure record at mooring A at 6.21 hours. (c) Low water phase lag between Sandy Hook and Mooring A.

the tidal month, the quarterdiurnal range varies by a factor of 4 (Fig. 5b). This is indicative of the quadratic, or nonlinear, relationship between the semidiurnal forcing and the generation of quarterdiurnal motion. One result of this modulation is a change in the low water time lag between Sandy Hook and the Navesink (Fig. 5c). During spring tides low water in the Navesink occurs 2.5 hours after low water at Sandy Hook. During neap tides the low water lag is only 1.5 hours. In contrast the high water lag is less than one hour (not shown).

Time series of pressure, velocity, salinity and turbidity at mooring A are plotted in Figure 6. Here, ebb velocities rarely exceed 20 cm/s, while flood velocities approach 50 cm/s (Fig. 6b). This inequality is in part driven by the tidal asymmetry, although the flood is also augmented by a mean flow. Record mean Eulerian flows are directed up estuary, consistent with gravitational circulation. During the first half of the record, following the high river discharge event, residual flows are 5–10 cm/s. During the second half the record subtidal flows decrease to below 5 cm/s.

As expected, salinities are low following the high river discharge event (Fig. 6c). The salinity on day 82 is under 14 psu and tends to increase up to day 91. As salinities rise following the discharge event they are marked by tidal period fluctuations. Tidal period fluctuations in salinity are largest between days 86 and 90 where they exceed 6 psu. These salinity fluctuations are consistent with enhanced horizontal salinity gradients during the

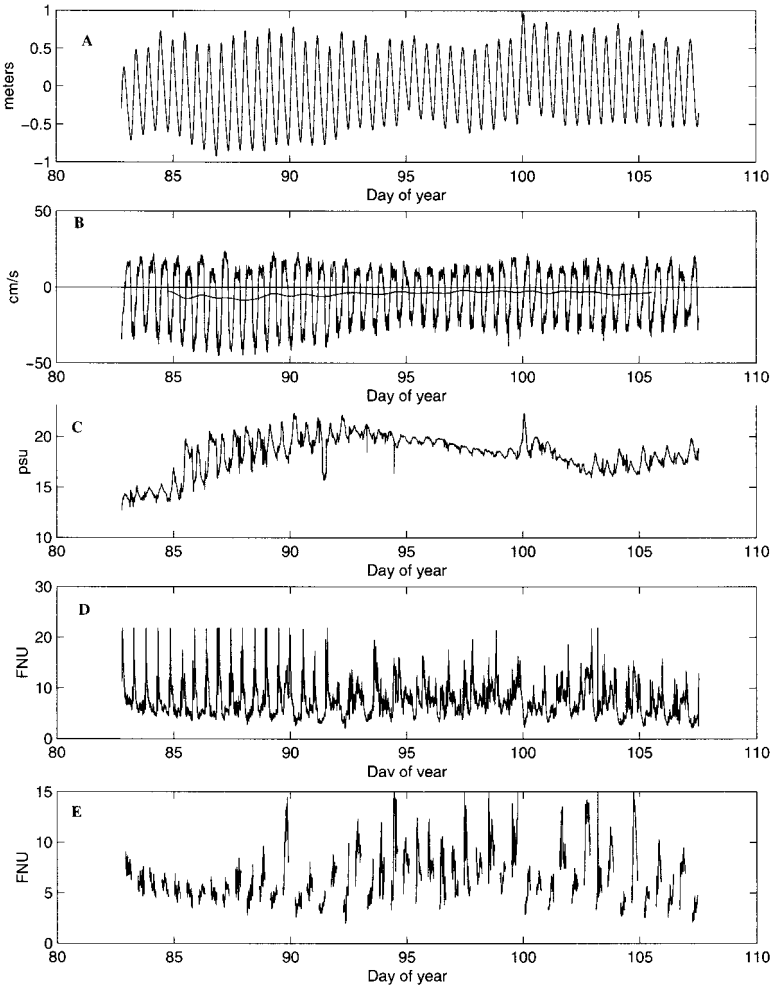

Figure 6. Time series obtained from mooring A. (A) Sea level (B) along channel current, low-passed along channel current and zero crossing (C) salinity (D) turbidity (E) turbidity plotted only during ebbing currents. The low-passed filter was a Lanczos filter with a half window width of 48 hours and a cutoff period of 32 hours.

first half of the record, suggesting that the stronger up-estuary flows during this time are driven by an enhanced baroclinic pressure gradient.

The turbidity record (Fig. 6d) is characterized by flood tide spikes during the first 10 days of the record, coinciding with spring tide conditions and enhanced stratification. Turbidity levels exceed the maximum range of the RCM9's turbidity sensor. Although the highest levels of turbidity occur during the flood prior to day 92, this same time period also coincides with low levels of turbidity during ebb (Fig. 6e). Thus the turbidity record during the spring tide is characterized by turbid waters during the flood and relatively clear waters throughout the ebb. This is consistent with the acoustic backscatter data obtained from the

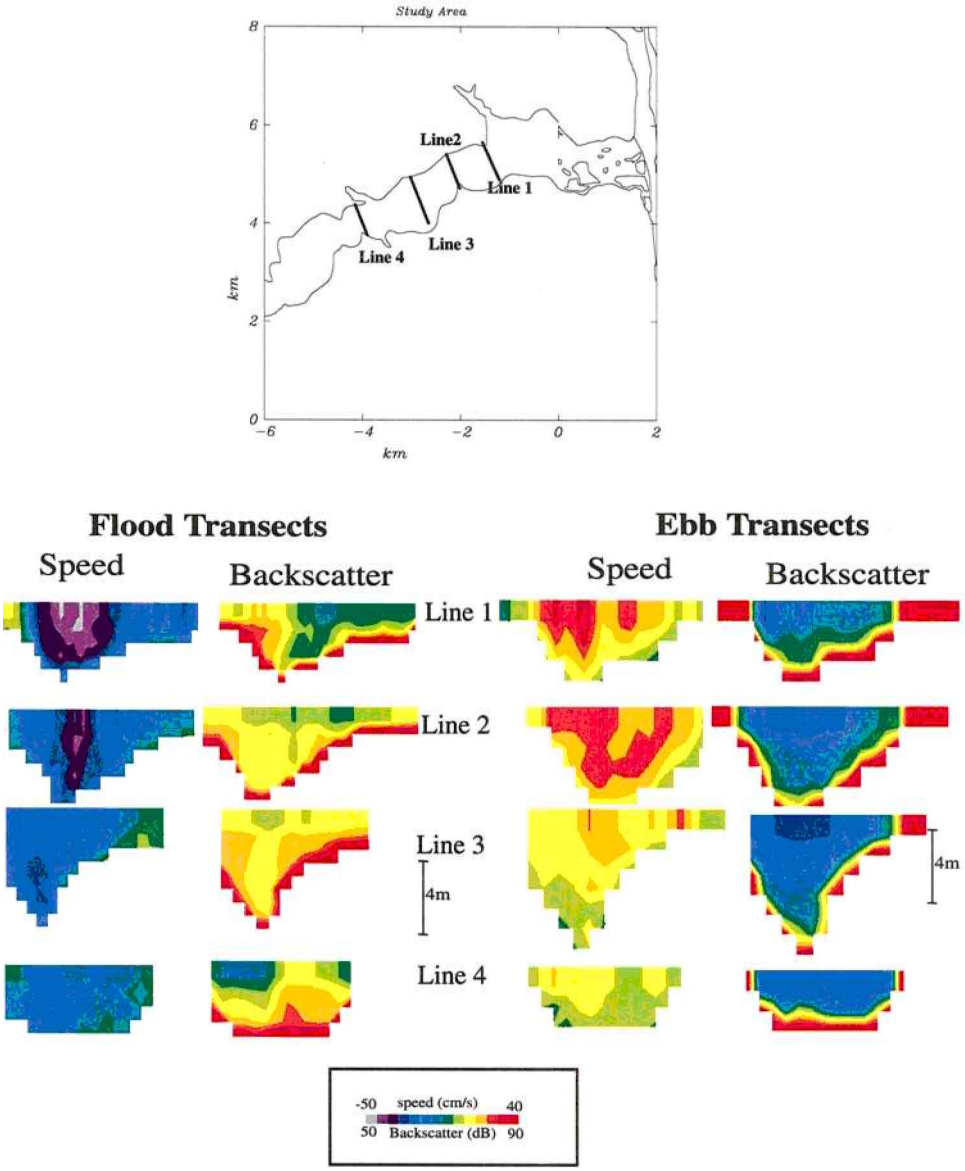

Figure 7. Backscatter intensity and along channel current speed during flood (left two panels) and ebb (right two panels). Vertical scale is shown. Locations of transects are shown in Figure 1. Perspective in these figures is looking seaward, i.e. north is to the left.

ADCP (Fig. 7), which we use as a proxy for the suspended load (Cheng *et al.,* 1997). Higher backscatter is evident on the flood, during which time appreciable lateral structure is evident. Lateral structure is most pronounced in the vicinity of a headland along line 2. During the flood, acoustic backscatter is highest along lines 1–3 and lower along line 4. On

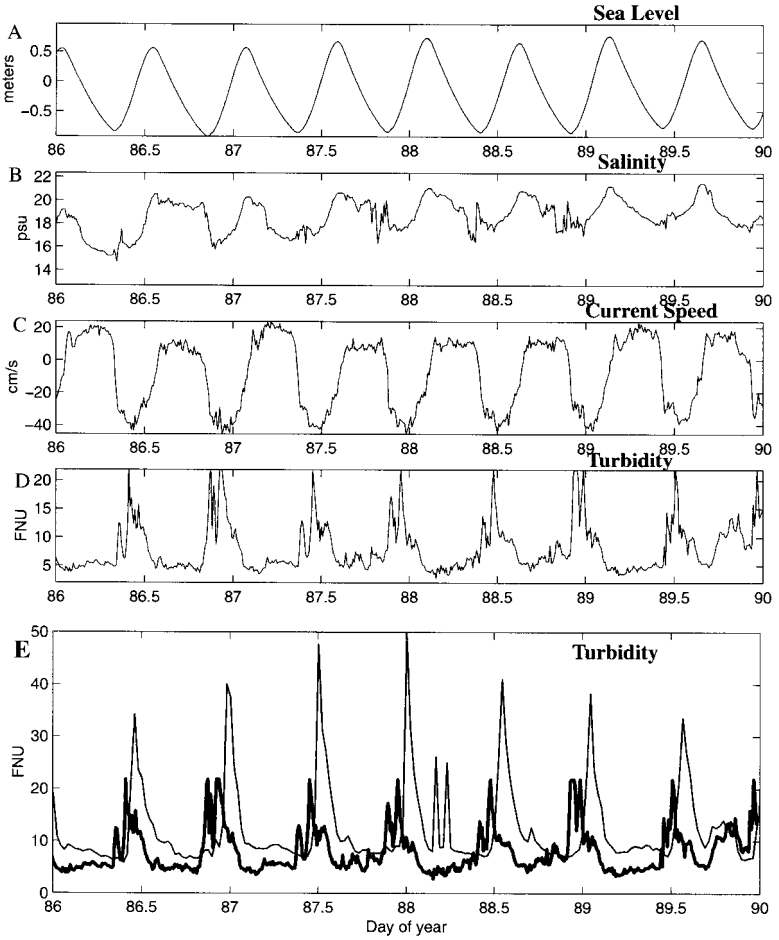

Figure 8. Close-up of data from mooring A: (A) sea level, (B) salinity, (C) along channel current speed, (D) turbidity, (E) overlay of turbidity at mooring A (thick line) and mooring B (thin line).

ebb, backscatter is lower and lateral gradients are weaker, particularly over the central channel.

A detailed look at moored data collected between days 86–90 is shown in Figure 8. Turbidity spikes on flood (Fig. 8d) are composed of multiple peaks, with each peak coinciding with rapid current accelerations. Current accelerations during flood tend to be step-like. After the initial acceleration into flood, current speed levels off for approximately 0.5 hr before accelerating further to maximum flood. (The salinity record indicates that these stepwise accelerations *are not* associated with the passage of a salt front.) Turbidity spike events occur during these accelerations. Note that following each resuspension event turbidity levels quickly drop off despite the continued strong currents. Turbidity spikes are also evident at mooring B (Fig. 8e). However, at this location a single smoother spike

occurs ~1.5 hours after the initial spike at mooring A. This time lag is consistent with the time to advect material between these two moorings, while the smearing of the multiple spikes suggests horizontal dispersion.

A peculiarity in the mooring data is a decline in salinity during the early flood. This is, however, consistent with CTD sections taken over a tidal cycle (Fig. 9). During the ebb (Fig. 9a) the water column becomes stratified as isohalines lay over. Stratification is strongest near the bottom at the end of the ebb where salty waters become isolated in deeper sections of the channel. Currents are strongly sheared across the halocline. In the surface layer currents exceed 40 cm/s, while below the halocline currents are weak, even during maximum ebb (middle panel Fig. 9a). As flood commences (Fig. 9b), the parcel of trapped salty water begins to move up estuary and the section is initially filled with fresher waters. However, as flood continues salinity levels eventually increase. Currents during the flood approach 50 cm/s near the surface. In the upper half of the water column vertical shears are weak. Vertical shear is evident near the bottom in the unstratified sections and below the halocline in the stratified region.

b. Modeling results

To more quantitatively discuss the interaction between buoyancy and tidal asymmetries a one-dimensional model was constructed. The governing equations for the model are:

$$\frac{\partial u}{\partial t} = -\frac{\partial}{\partial z}\left(A_v \frac{\partial u}{\partial z}\right) - \frac{g}{\rho}\frac{\partial \rho}{\partial x} z \tag{1}$$

$$\frac{\partial S}{\partial t} = -\frac{\partial}{\partial z}\left(A_D \frac{\partial S}{\partial z}\right) - u\frac{\partial S}{\partial x} \tag{2}$$

$$\frac{\partial C}{\partial t} = -\frac{\partial}{\partial z}\left(A_D \frac{\partial C}{\partial z}\right) - w_s \frac{\partial C}{\partial z} \tag{3}$$

where, u is the current speed, S is salinity, C is the concentration of a passively settling tracer, A_V and A_D are the vertical eddy viscosities and diffusivities, t is time, x and z are the along-estuary and vertical dimensions. The model is forced by prescribing the depth-averaged current, which was estimated by a least-squares fit of a semidiurnal, quarterdiurnal and sixthdiurnal signals to depth-averaged ADCP data collected in the vicinity of mooring A. Vertical mixing coefficients were calculated using the Mellor and Yamada level 2.5 turbulent closure scheme (Mellor and Yamada, 1982). Boundary conditions are zero flux of salt and tracer through the surface and bottom grid. Bottom stress was specified via the law of the wall with $z_0 = 1$ mm (Friedrichs and Wright, 1997).

Eq. 1 is a form of the momentum equation used to calculate vertical shear. Eq. 2 is a salt equation and Eq. 3 describes the changing concentration of a passively settling tracer subject to vertical mixing. In Eq. 1, the term on the left-hand side is the local acceleration of along-channel current. The first term on the right-hand side of Eq. 1 represents the

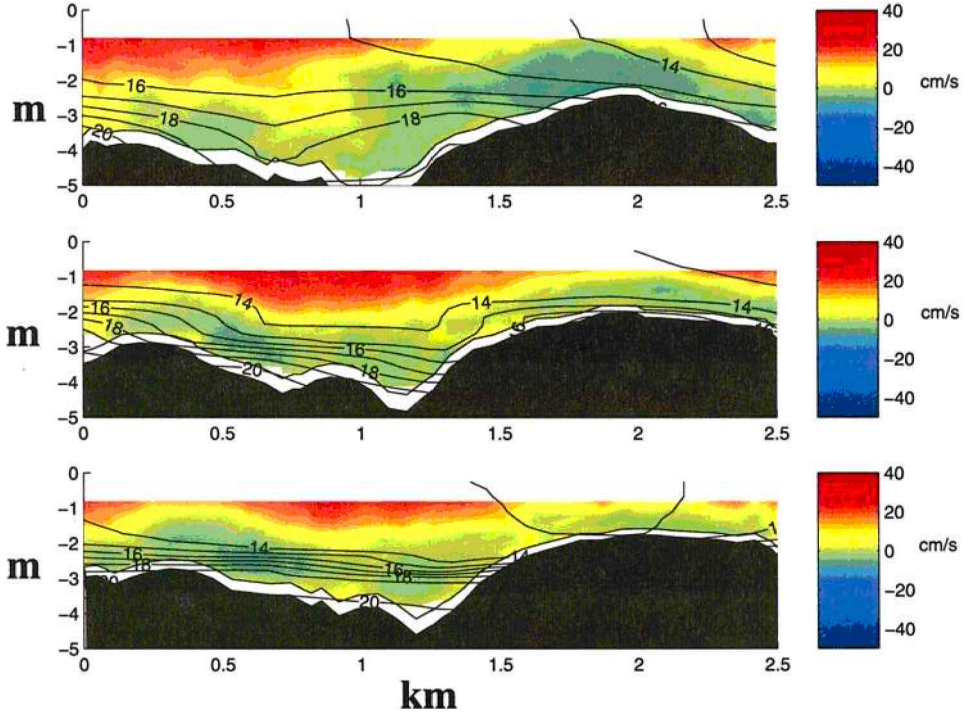

Figure 9. (a) Salinity—psu (contour) and along channel current speeds—cm/s (color) during three consecutive transects taken during the ebb on March 27, corresponding to Year Day 86. The three transects were run at 14:37, 16:24 and 18:00 GMT.

vertical stress divergence and the second term is the baroclinic pressure gradient due to a prescribed depth independent horizontal density gradient. In Eq. 2, the term on the left-hand side is the local time rate of change in salinity. The first term on the right-hand side represents vertical mixing of salt, while the second term is the horizontal advection of the prescribed salinity gradient. In Eq. 3, the term on the left-hand side represents the local time rate of change of a passively settling tracer. The first term on the right-hand side is the vertical mixing of the tracer, and the second term reflects settling.

The second term on the rhs in all three equations require specified parameters. Eqs. 1 and 2 require specification of a horizontal salinity gradient, while Eq. 3 requires a value for w_s. In all simulations the tracer settles downward at a constant rate of 1 mm/s ($w_s = -1$ mm/s) and is initially well mixed in the vertical. Model runs are made to assess the sensitivity of the solution to changes in the horizontal density gradient.

Eqs. 1–3 are cast into a finite difference scheme with 20 staggered grids in the vertical in 5 meters of water, to represent the depth at mooring A. Three simulations are presented with varying horizontal salinity gradients. Simulations are run for three days with only the last day presented. In all cases the model reached steady state by the second day.

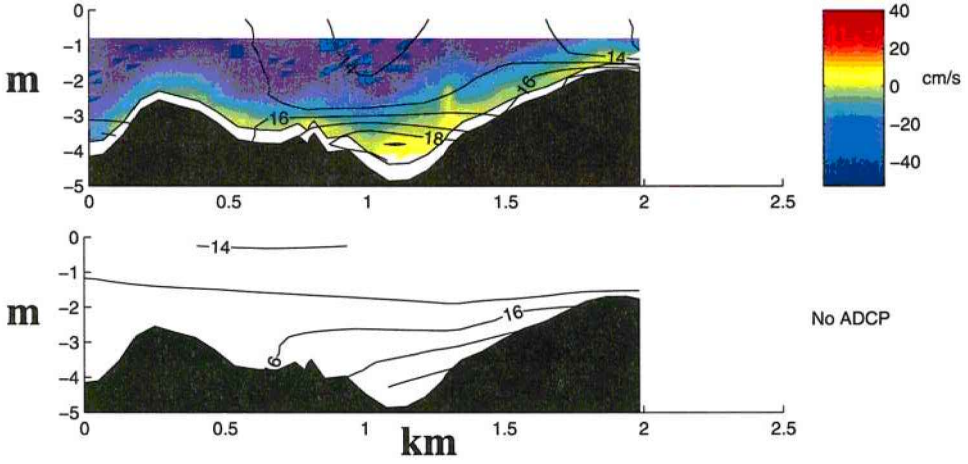

Figure 9. (b) Salinity sections on two consecutive transects taken during the flood on March 27, corresponding to Year Day 86. These two transects were run at 21:58 and 22:30 GMT.

Results from a simulation with zero salinity gradient are presented in Figure 10a. The prescribed flood-dominance is evident in the current velocity. During the long slow ebb, current speeds reach 32 cm/s, while on flood they reach 58 cm/s. Vertical diffusivities reflect the tidal asymmetry in current speed. Vertical eddy viscosity during the flood approaches .01 m^2/s, approximately twice the value on the ebb. Tracer concentration exhibits some tidal asymmetry. During the flood, material is mixed higher in the water column than on the ebb. At slack water there is a decline of material near the surface and a corresponding increase near the bed. However, during both phases of the tide the tracer is appreciably mixed throughout the water column.

Results from a second simulation, with a prescribed horizontal salinity gradient of 0.5 psu/km, are presented in Figure 10b. Currents here are similar to those in the run with zero salinity gradient, with some minor, but telling differences. Maximum currents of 57 cm/s during the flood are slightly weaker than the previous run. In contrast, maximum currents during ebb of 35 cm/s are slightly stronger than those in the previous simulation. Since depth-averaged currents are the same in the two runs, the difference in the depth-dependent current is due to a change in the vertical shear. During the flood vertical shears are slightly weaker and on the ebb they are stronger. This occurs due to the straining of the salinity gradient by the vertical shear. On the ebb, vertical shears tend to stratify the water column, which reduces vertical mixing, supports stronger vertical shear and yields stronger surface current speeds. In contrast, on flood, overstraining of the density gradient augments vertical mixing, which weakens vertical shears and reduces surface current speeds. The difference between these two simulations is most apparent in the vertical eddy diffusivities, which are nearly three times higher on the flood than on the ebb.

In the second simulation enhanced tidal period asymmetry in tracer concentration is evident. Suspended material during ebb resides lower in the water column, and during

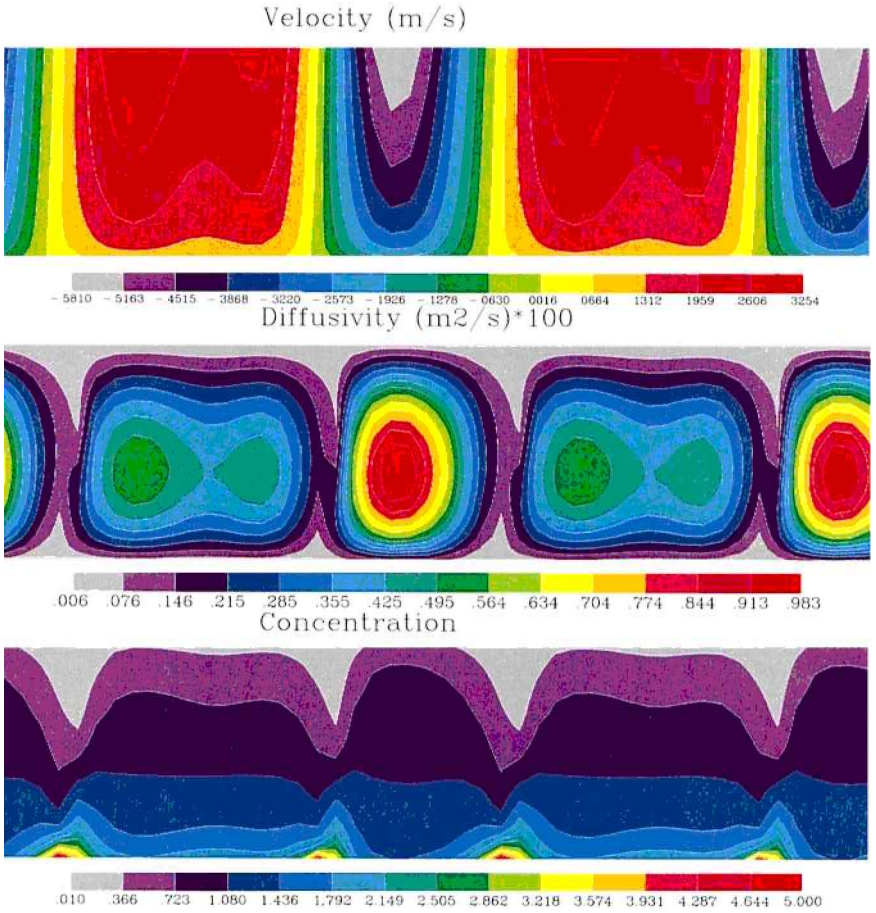

Figure 10(a). Results from numerical simulation with zero prescribed horizontal density gradient. Top panel shows current speed. Ebbing currents are red. Middle panel plots turbulent eddy diffusivity and the lower panel plots concentration of a tracer with a settling velocity of 1 mm/s.

slack water higher concentrations are evident near the bottom. In the upper half of the water column there is some weak stratification during the ebb, through slack, and into early flood. The suspended material is capped by this stratification. During flood, mixing of suspended material occurs in discrete steps. However, despite these slight differences, overall results from these two simulations are very similar, because the water column is generally well mixed throughout most of the tidal cycle.

Finally, a third run is presented with a horizontal salinity gradient of 1 psu/km (Fig. 10c). This simulation differs dramatically from the previous two runs. In particular, the water column becomes vertically stratified during the ebb and well mixed on the flood. This strong tidal period asymmetry is due to the synergistic tendencies of barotropic tidal asymmetries and tidal straining. Flood turbulence, generated by stronger tidal currents, acts

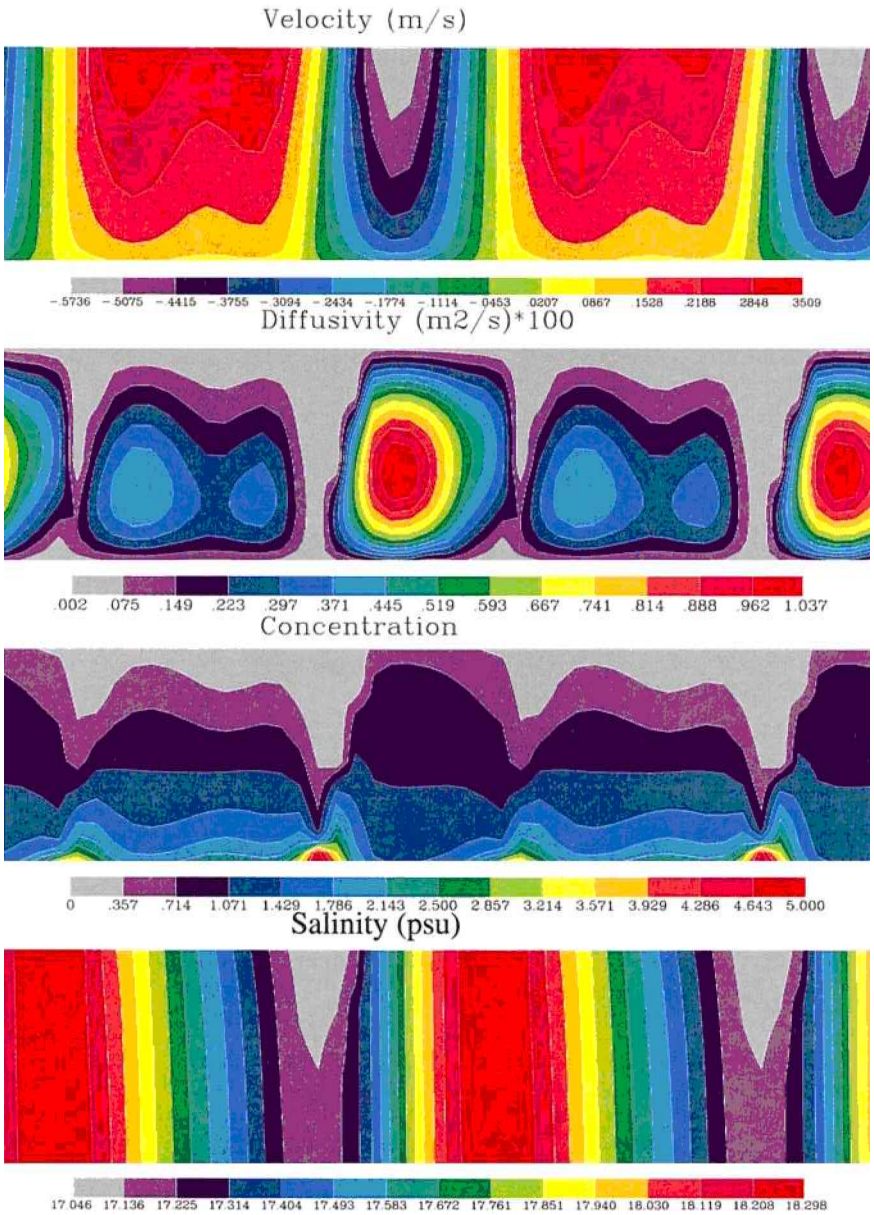

Figure 10. (b) Results from numerical simulation with a prescribed horizontal salinity gradient of 0.5 psu/km. Top panel shows current speed. Ebbing currents are red. Second panel plots turbulent eddy diffusivity. The third panel plots concentration of a tracer with a settling velocity of 1 mm/s. The fourth panel plots the salinity.

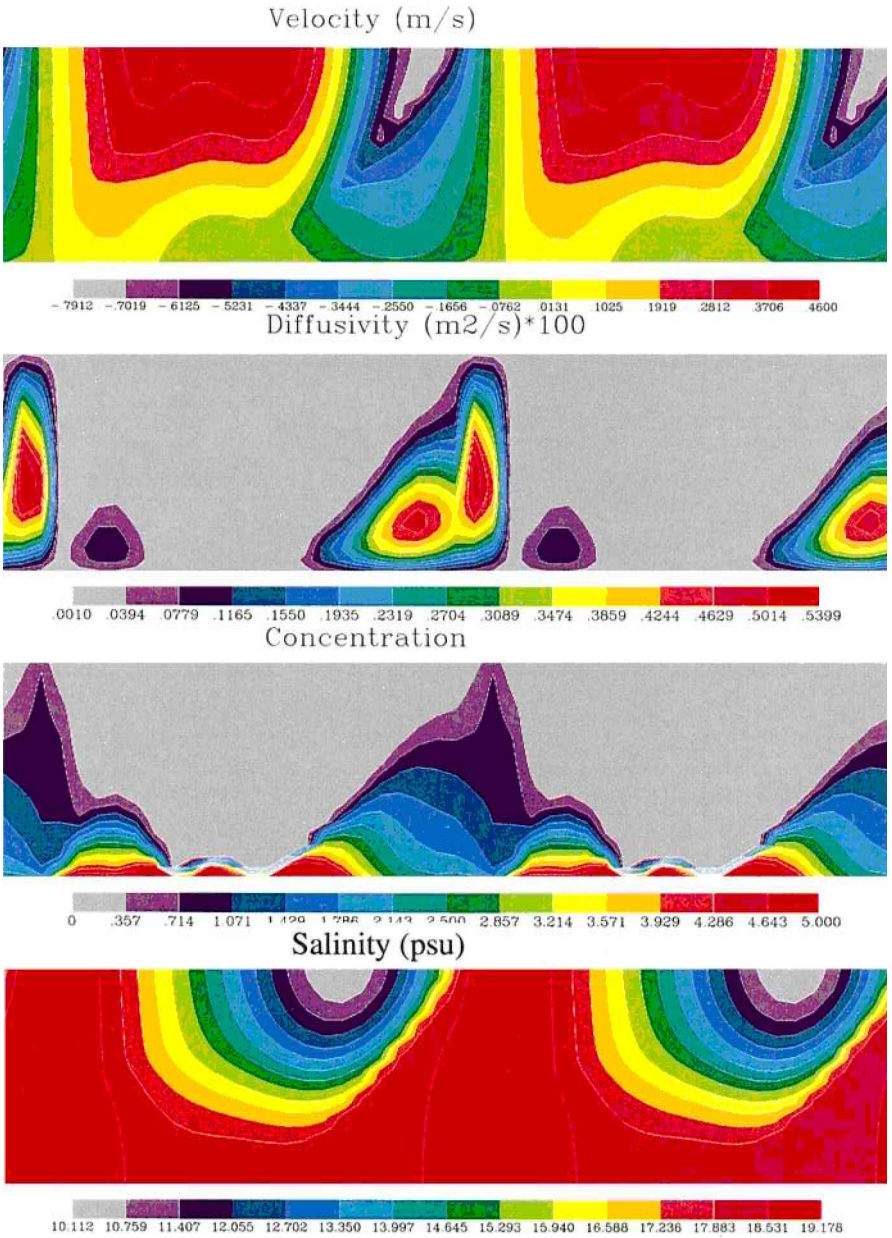

Figure 10. (c) Results from numerical simulation with a prescribed horizontal salinity gradient of 1.0 psu/km. Top panel shows current speed. Ebbing currents are red. Second panel plots turbulent eddy diffusivity. The third panel plots concentration of a tracer with a settling velocity of 1 mm/s. The fourth panel plots the salinity.

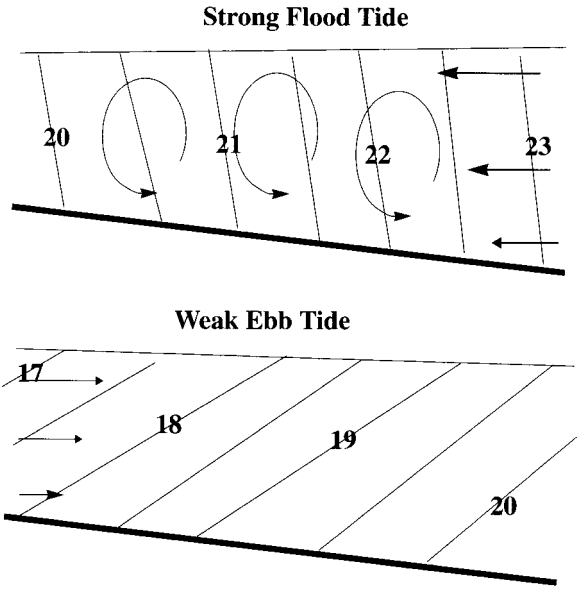

Figure 11. Upper panel shows schematic of "overstraining" of the density field by vertical shears on the flood. Lower panel shows stratifying effect of straining of the density field by vertical shear on the ebb.

in concert with overstraining of the salt field (Neph and Geyer, 1996) to homogenize the water column. In contrast, on the long but weak ebb, vertical mixing is shut off allowing isohalines to gently lay over and stratify the water column.

The tidal asymmetry in vertical mixing profoundly affects the transport of the passively settling tracer. When mixing is turned off during the ebb, suspended matter sinks to the bottom (where in the numerical model it collects in the bottom grid point that encompasses the first 25 cm above the bottom). During flood, mixing transports suspended matter into the water column, where it would be advected upstream. Since the material is of a limited source, however, concentrations in the lower third of the water column tend to reach a maximum during early flood, after which concentrations decrease as the material is mixed throughout the water column. In general, the third simulation is consistent with many features we have described in the field data.

5. Discussion and conclusions

Our results suggest that the particle trapping tendencies of a flood-dominated system are augmented following times of high river discharge. The intensified trapping occurs because the barotropic tidal asymmetry heightens tidal period asymmetries in stratification. The coupling between the barotropic and baroclinic tidal asymmetries is summarized in the schematic shown in Figure 11. During the ebb, vertical shear advects light water over

heavy water, producing stable stratification. This process is referred to as straining. In contrast, during the flood, vertical shears tend to advect heavy water over light water, producing an unstable stratification which drives vertical mixing. Neph and Geyer (1996) refer to this latter process as ''over-straining.'' The tendency for tidal straining to produce this tidal period asymmetry in stratification was discussed previously (Jay and Smith, 1990; Geyer *et al.,* 2000; Neph and Geyer, 1996; Simpson *et al.,* 1990). However, this study demonstrates that tidal asymmetries in stratification due to straining are enhanced in flood-dominated systems. The long slow ebb is an effective stratifying mechanism because current speeds during ebb are insufficient to drive vertical mixing resulting in a pure straining motion. In contrast, on flood, vertical mixing resulting in turbulence generated by the strong flood is augmented by overstraining of the salinity field, and stratification is destroyed.

The tidal period asymmetries in vertical mixing drive tidal period variability in resuspension and deposition, which controls turbidity levels in this shallow-stratified estuary. While this intratidal behavior is consistent with Wellerhaus (1981) and Lang *et al.* (1989), results presented here emphasize that tidal period asymmetries in resuspension and deposition are heightened in a stratified flood-dominated estuary. These asymmetries drive a net landward transport of suspended matter and may play an important role in the sorting of material. Furthermore, tidal period variability in turbidity levels presents the biota with a dynamic environment where light level and visibility, availability of suspended foods, predator-prey interactions, and other ecological parameters and functions change with the time-varying turbidity field. While Burchard and Baumert (1998) suggest that tidal period variability in mixing is not required to maintain a turbidity maximum, tidal period variability in the suspended load observed in this study and others (Lang *et al.,* 1989; Friedrichs *et al.,* 2000) could not be replicated without tidal period variability in vertical mixing.

In shallow systems, such as the Navesink, tidal period resuspension and deposition are important processes controlling the dynamics of the suspended load for three reasons. First, suspended matter falling at 1 mm/s will transverse the entire water column in a fraction of a tidal cycle. Thus, as turbulence is shut down during the long, slow, stratified ebb, suspended matter falls to the bottom. Secondly, the barotropic tidal wave becomes highly distorted in shallow systems leading to strong tidal period asymmetries in bottom stress and vertical mixing. Thirdly, this asymmetry is augmented by tidal straining of the horizontal density gradient. Together, these processes produce appreciable tidal period variations in the suspended load such that the transport of material is likely to be primarily due to this asymmetry, rather than that associated with the weak gravitational circulation in shallow estuaries.

This tidal period asymmetry in vertical mixing can explain the observed peaks in turbidity. During the ebb, vertical mixing is reduced by the stratification. Consequently, material suspended in the water column settles downward. Currents at the surface during

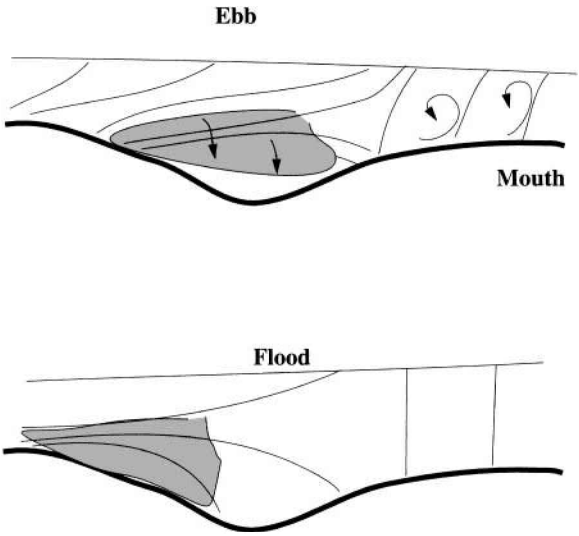

Figure 12. Schematic showing trapping mechanism in stratified flood dominated estuary. Upper panel depicts settling of suspended matter over length scale L during the ebb. Lower panel shows resuspension of this material during the flood.

the ebb are less than 30 cm/s, corresponding to approximately 1 km/hour. If turbulence in the stratified water column were completely shut down, a particle with a settling velocity of 0.25 mm/s would descend 4 meters in 3 hours and remain in the estuary because it would reach the bottom. On flood the water column becomes well mixed, and this material is resuspended and advected landward. A schematic of this process is presented in Figure 12. Furthermore, this scenario may produce turbidity spikes because only the limited amount of material deposited during ebb is readily available to be resuspended on the following flood.

Resuspension events at mooring A during the flood are characterized by multiple distinct spikes occurring simultaneously with step-wise current accelerations. This timing suggests that the resuspension events occur at or near the seaward mooring, and that the double spiked event could be due to limited, but multiple, layers of erodible material. Limited layers of easily erodible material have been documented to exist in other estuarine systems (Bokuniewicz *et al.,* 1975). At mooring B, which resides up estuary, a single but more diffuse turbidity spike occurs. The timing of this spike is consistent with the advective time-scale between the moorings, while the diffused nature of the turbidity signal reflects horizontal dispersion of the suspended material as it is advected upstream.

To estimate an effective horizontal diffusion coefficient, with dimensions of length squared over time, we need representative length and time scales. For a length scale (L) we choose $L = u^*\Delta t$ where u is characteristic of the flood tide velocity (35 cm/s) and Δt is the time between multiple turbidity spikes at mooring A, approximately 0.5 hours. This length

scale represents the distance that the first resuspension event has advected up estuary at the time of the second turbidity spike. Thus $L \sim 600$ m. Horizontal diffusion smears these spikes together in the 1.5 hours it takes to reach the second mooring. This time represents an upper limit on the diffusion time, or equivalently a lower limit on the effective horizontal dispersion. Thus $T \sim 1.5$ hr. These time and length scales place the lower limit of horizontal dispersion (L^2/T) at ~ 75 m^2/s. This estimate is reasonable in light of estimates made in other systems (Wilson and Okubo, 1978; Zimmerman, 1986).

One could conclude that these flood tide resuspension events are filling this estuary. However, if the resuspension events are primarily composed of fluffy, organically-rich material, accumulation rates would be reduced by decomposition, and this would explain the high levels of organics found in the Navesink. Furthermore, enhanced trapping may only occur following times of high river discharge. During lower flow and no flow events, tidal asymmetries in vertical mixing would not be as pronounced. Consequently, the tendency for material to be trapped during high flow events may be countered by dispersion during low flow events. If the tidal excursion is of the same length scale as the coastline irregularities, as it is in the Navesink, strong dispersive tendencies are likely (Okubo, 1973; Zimmerman, 1986). Consequently, the distribution of suspended matter may never reach equilibrium, but rather tends to disperse during low discharge events and concentrate during high discharge events.

Physical processes affecting transport of sediments may also influence the transport of planktonic and small, demersal animals. For example, some polychaete larvae behave essentially as passive particles (Hannan, 1984), and the physical model for particulate transport in the Navesink River estuary may provide important insights into polychaete recruitment in this and other systems. In fact, in 1997 the highest densities of both polychaetes and bivalves in the Navesink were found in the middle reaches of the River (NMFS, unpubl. data). Seasonal and interannual variations in stratification and particulate transport may have important biological consequences and should be considered in future analysis of benthic recruitment. In particular, details in the timing between critical larval stages and enhanced particle trapping may significantly influence the spatial structure and success of recruitment. However, the transport of planktonic animals is complicated by the fact that most are capable of responding to physical gradients and demonstrate at least some form of vertical migration (Forward, 1988). The effects of vertical migration on estuarine transport are well known and have been modeled (Smith and Stoner, 1993; Hill, 1998).

While both observations and numerical simulations elucidate how the interplay between barotropic tidal asymmetries and buoyancy augments particle trapping in flood dominated systems, other processes, however, are likely to modify this mechanism such as effects of along channel gradients in tidal energy, and effects of lateral variability. Acoustic backscatter data suggest both of these are at play. A sudden drop in acoustic backscatter between lines 3 and 4 during the flood suggests a depositional region. Lateral structure is

apparent in all sections and appears to be enhanced during the flood. Tidal period asymmetries in lateral structure have been shown to produce cross-channel gradients in sedimentation rates (Geyer *et al.,* 1998). These same physical processes, coupled with either passive settling larvae or larvae with tidal period behavior, may also provide mechanisms generating cross-channel gradients in larval settlement. These are some of the issues that will be addressed in future work.

Acknowledgments. Numerous scientists from NFMS Sandy Hook and Rutgers University participated in this project. In particular we thank John Manderson, John Rosendale and Allen Bejda from the NMFS lab for their enthusiastic and tireless efforts in the lab and in the field. RJC acknowledges support from the Rutgers/NOAA Cooperative Marine Education and Research Program (NA67FE0381) of the U.S. Department of Commerce's National Oceanic and Atmospheric Administration under Grant # NA76-RG0091. This is IMCS Contribution No. 2001–2.

REFERENCES

Aubrey, D. G. and P. E. Speer. 1985. A study of non-linear tidal propagation in shallow inlet/estuarine systems, Part I: Observations. Estuar. Coast. Shelf Sci., *21,* 185–205.

Bokuniewicz, H. J., R. B. Gordon and D. C. Rhoads. 1975. Mechanical properties of the sediment-water interface. Mar. Geol., *18,* 263–278.

Burchard, H. and H. Baumert. 1998. The formation of estuarine turbidity maxima due to density effects in the salt wedge: A hydrodynamic process study. J. Phys. Oceanogr., *28,* 309–321.

Cheng, R. T., J. W. Gartner and R. E. Smith. 1997. Bottom boundary layer in South San Francisco Bay California. J. Coast. Res., *25,* 49–62.

Forward, R. B., Jr. 1988. Diel vertical migration: Zooplankton photobiology and behaviour. Oceanogr. Mar. Biol. Ann. Rev., *26,* 361–393.

Friedrichs, C. T. and D. G. Aubrey. 1988. Non-linear tidal distortion in shallow well-mixed estuaries: A synthesis. Estuar. Coast. Shelf Sci., *27,* 521–545.

Friedrichs, C. T. and O. S. Madsen. 1992. Nonlinear diffusion of the tidal signal in frictionally dominated embayments. J. Geophys. Res., *97,* 5637–5650.

Friedrichs, C. T., M. E. Scully, G. M. Battisto and L. C. Schaffner. 2000. Sediment transport associated with tidal asymmetry in stratification, mixing and resuspension in the York River Estuary, *in* Proceedings of the 10th International Biennial Conference on Physics of Estuaries and Coastal Seas, SRAMSOE Report No. 366, C. T. Friedrichs and A. Valle-Levinson, eds., Virginia Institute of Marine Science, Gloucester Point, VA, 214–216.

Friedrichs, C. T. and L. D. Wright. 1997. Sensitivity of bottom stress and bottom roughness estimates to density stratification, Eckernförd Bay, southern Baltic Sea. J. Geophys. Res., *102,* 5721–5732.

Geyer, W. R. 1993. The importance of suppression of turbulence by stratification on the estuarine turbidity maximum. Estuaries, *16,* 113–125.

—— 1997. Influence of wind on dynamics and flushing of shallow estuaries. Estuar. Coast. Shelf Sci., *44,* 713–722.

Geyer, W. R., R. P. Signell and G. C. Kineke. 1998. Lateral trapping of sediment in a partially mixed estuary, *in* Physics of Estuaries and Coastal Seas, J. Dronkers and M. Scheffers, eds., Balkema Rotterdam, 115–126.

Geyer, W. R., J. H. Trowbridge and M. M. Bowen. 2000. The dynamics of a partially mixed estuary. J. Phys. Oceanogr., *30,* 2035–2048.

Hamblin, P. F. 1989. Observations and model of sediment transport near the turbidity maximum of the upper Saint Lawrence Estuary. J. Geophys. Res., *94,* 14381–14405.

Hannan, C. A. 1984. Planktonic larvae may act like passive particles in turbulent near-bottom flows. Limnol. Oceanogr., *29,* 1108–1116.

Hill, A. E. 1991. Vertical migration in tidal currents. Mar. Ecol. Prog. Ser., *75,* 39–54.

—— 1994. Horizontal zooplankton dispersal by diel vertical migration in S-2 tidal currents on the northwest European continental shelf. Cont. Shelf Res., *14,* 491–506.

—— 1998. Diel vertical migration in stratified tidal flows: Implications for plankton dispersal. J. Mar. Res., *56,* 1069–1096.

Jay, D. A. and J. D. Musiak. 1994. Particle trapping in estuarine tidal flows. J. Geophys. Res., *99,* 445–461.

Jay, D. A. and J. D. Smith. 1990. Residual circulation in shallow estuaries 1. Highly stratified, narrow estuaries. J. Geophys. Res., *95,* 711–731.

Lang, G., R. Schubert, M. Markofsky, H. U. Fanger, I. Grabemann, H. L. Krasemann, L. J. R. Newmann and R. Riethmüller. 1989. Data interpretation and numerical modeling of the mud and suspended sediment experiment 1985. J. Geophys. Res., *94,* 14381–14405.

Linden, P. F. and J. E. Simpson. 1988. Modulated mixing and frontogensis in shallow seas and estuaries. Cont. Shelf Res., *8,* 1107–1127.

Mellor, G. L. and T. Yamada. 1982. Development of a turbulence closure model for geophysical fluid problems. Rev. Geophys. Space Phys., *20,* 851–875.

Neph, H. M. and W. R. Geyer. 1996. Intra-tidal variations in stratification and mixing in the Hudson Estuary. J. Geophys. Res., *101,* 12079–12086.

Officer, C. B. 1981. Physical dynamics of estuarine suspended sediment. Mar. Geol., *40,* 1–14.

Okubo, A. 1973. Effect of shoreline irregularities on streamwise dispersion in estuaries and other embayments. Neth. J. Sea Res., *6,* 213–224.

Peters, H. and R. Bokhorst. 2000. Microstructure observations of turbulent mixing in a partially mixed estuary. Part I: Dissipation rate. J. Phys. Oceanogr., *30,* 1232–1244.

Rhoads, D. C. 1973. The influence of deposit-feeding benthos on water turbidity and nutrient recycling. Am. J. Sci., *273,* 1–22.

Rhoads, D. C., L. F. Boyer, B. L. Welsh and G. R. Hampson. 1984. Seasonal dynamics of detritus in the benthic turbidity zone (BTZ): Implications for bottom-rack molluscan mariculture. Bull. Mar. Sci., *35,* 536–549.

Rhoads, D. C. and D. K. Young. 1970. The influence of deposit-feeding benthos on bottom stability and community trophic structure. J. Mar. Res., *28,* 150–178.

Schubel, J. R. 1968. Turbidity maximum of the northern Chesapeake Bay. Science, *6,* 1012–1015.

Schubel, J. R. and D. W. Pritchard. 1972. The estuarine environment, Pt. 1, Council on Education in the Geological Sciences, J. Geol. Education., *20,* 60–68.

Simpson, J. H., J. Brown, J. Matthews and G. Allen. 1990. Tidal straining, density currents and stirring in the control of estuarine stratification. Estuaries, *13,* 125–132.

Smith, N. P. and A. W. Stoner. 1993. Computer simulation of larval transport through tidal channels: Role of vertical migration. Estuar. Coastal Shelf Sci., *37,* 43–58.

Speer, P. E. and D. G. Aubrey. 1985. A study of non-linear tidal propagation in shallow inlet/estuarine systems, Part II: Observations. Estuar. Coast. Shelf Sci., *21,* 207–222.

Wellerhaus, S. 1981. Turbidity maximum and mud shoaling in the Weser Estuary. Arch. Hydrobiol., *92,* 14395–14405.

Wilson, R. E. and A. Okubo. 1978. Longitudinal dispersion in a partially mixed estuary. J. Mar. Res., *36,* 427–447.

Young, D. K. and D. C. Rhoads. 1971. Animal-sediment relations in Cape Cod Bay, Massachusetts I. A transect study. Mar. Biol., *11,* 242–254.

van Aken, H. M. 1986. Onset of seasonal stratification in shelf seas due to differential advection. Cont. Shelf Res., *5,* 475–485.

Zimmerman, J. T. F. 1986. The tidal whirlpool: A review of horizontal dispersion by tidal and residual currents. Neth. J. Sea Res., *20,* 133–154.

Received: *27 July, 2000;* revised: *17 November, 2000.*